Accretion Disk Luminosity for Black Holes Surrounded by Dark Matter with Anisotropic Pressure

E. Kurmanov[1,2], K. Boshkayev[1,2,3] , R. Giambò[4,5], T. Konysbayev[1,2], O. Luongo[1,4,6], D. Malafarina[3] , and H. Quevedo[2,7,8]

[1] National Nanotechnology Laboratory of Open Type, Almaty 050040, Kazakhstan; kurmanov.yergali@kaznu.kz, kuantay@mail.ru, talgar_777@mail.ru, orlando.luongo@unicam.it

[2] Al-Farabi Kazakh National University, Al-Farabi Ave. 71, 050040 Almaty, Kazakhstan; quevedo@nucleares.unam.mx

[3] Department of Physics, Nazarbayev University, Kabanbay Batyr 53, 010000 Nur-Sultan, Kazakhstan; daniele.malafarina@nu.edu.kz

[4] Scuola di Scienze e Tecnologie, Università di Camerino, Via Madonna delle Carceri 9, I-62032 Camerino, Italy

[5] Istituto Nazionale di Fisica Nucleare, Sezione di Perugia, Via Alessandro Pascoli 23c, I-06123 Perugia, Italy

[6] Dipartimento di Matematica, Università di Pisa, Largo B. Pontecorvo 5, Pisa, I-56127, Italy

[7] Instituto de Ciencias Nucleares, Universidad Nacional Autónoma de México, Mexico

[8] Dipartimento di Fisica and ICRA, Università di Roma "La Sapienza", Roma, Italy

Received 2021 November 3; revised 2021 December 1; accepted 2021 December 9; published 2022 February 7

Abstract

We investigate the luminosity of the accretion disk of a static black hole surrounded by dark matter with anisotropic pressure. We calculate all basic orbital parameters of test particles in the accretion disk, such as angular velocity, angular momentum, energy, and radius of the innermost circular stable orbit as functions of the dark matter density, radial pressure, and anisotropic parameter, which establishes the relationship between the radial and tangential pressures. We show that the presence of dark matter with anisotropic pressure makes a noticeable difference in the geometry around a Schwarzschild black hole, affecting the radiative flux, differential luminosity, and spectral luminosity of the accretion disk.

1. Introduction

The common disk-like particle flow lying around compact objects, dubbed the accretion disk, permits the direct observation of the radiation emitted by the orbiting material rotating in the gravitational field of an astronomical object (Ho et al. 1997; Richstone et al. 1998; Abramowicz & Fragile 2013). In particular, the corresponding spectra are commonly observed, and so, as the accreting material fuels the region around the central object, observers can extract information about the properties of the whole system (Abramowicz et al. 1988). For extremely compact objects, the relativistic effects are clearly nonnegligible. On the one hand, the luminosity itself can be described simply by some emission spectrum model; however, on the other hand, the motion of particles in the disk and the trajectory of light rays escaping the disk require Einstein's field equations. Thus, the exterior geometry of the accretor, namely the central object, can be modeled through a metric with a given symmetry, which will determine the properties of the observed radiation (Shapiro & Teukolsky 1983; Torres 2002; Boshkayev et al. 2021b). In this picture, one can investigate not only black holes, white dwarfs, neutron stars, quasars, radio galaxies, and X-ray binaries, but also more exotic, hypothetical objects, e.g., boson stars (Torres 2002; Guzmán 2006) or gravastars (Mazur & Mottola 2004; DeBenedictis et al. 2006).

The central object's mass grows through accretion, and to fully describe the disks, one requires an exterior configuration and then solves the hydrodynamic equilibrium equations (Hartle & Thorne 1968; Paschalidis & Stergioulas 2017). Frequently, "exotic" matter contributions seem to be needed to describe hypothetical objects that are massive and compact, in order to fulfill stability criteria. Analogous examples can often be found in the case of wormholes and for cosmological backgrounds[9] (Copeland et al. 2006; Luongo & Muccino 2018; Capozziello et al. 2021).

In this work, we consider a static spherically symmetric configuration composed of a central black hole surrounded by a dark matter envelope. The gravitational field in the vacuum region around the black hole is described by the exterior Schwarzschild spacetime while the corresponding dark matter distribution, located at a given distance from the black hole, and its properties, is described by making use of the Tolman–Oppenheimer–Volkoff (TOV) equations.

We assume that the dark matter envelope does not interact with the baryonic matter of the accretion disk that is located within the envelope itself. We then apply the theory of black hole accretion developed in Novikov & Thorne (1973) for astrophysical black hole candidates in order to model the emitted spectrum from the accretion disk. In particular, we aim to test the consequences of two main assumptions: (i) first, dark matter endowed with a nonvanishing radial pressure term entering the TOV equations, namely $P_r(r) = P(r)$, and (ii) second, the energy-momentum tensor being anisotropic, leading to an additional pressure term, which is interpreted as a nonvanishing tangential pressure, $P_\theta(r)$. We physically motivate these two choices and characterize the dark matter distribution accordingly by computing the difference $P_\theta(r) - P(r)$.

---

[9] In general, above all in cosmological scenarios, exotic matter could indicate that general relativity breaks down (Capozziello et al. 2019). There is no general agreement about the possible existence of exotic matter, namely matter whose equation of state is not ordinary (Dai & Stojkovic 2019). However, this goes beyond the purpose of our work.

It should be stressed that the theory of anisotropic fluids is well known in the literature. In particular, it has been shown that anisotropic fluids may be geodesic in general relativity by Herrera et al. (2002). A general study of spherically symmetric dissipative anisotropic fluids is given in Herrera et al. (2004). Exact static spherically symmetric anisotropic solutions of the field equations are obtained and analyzed in Bayin (1982) and Herrera et al. (2008). Anisotropic stars in general relativity and their mass–radius relations are computed in Mak & Harko (2003). In this work, we instead study the effects of dark matter with anisotropic pressures on test particles in the accretion disk present within the dark matter and the spectra of the disk. In particular, we compare the motion of particles and the accretion disk's spectra with the cases of isotropic dark matter and a Schwarzschild black hole in vacuum.

This paper is organized as follows: In Section 2, we describe a configuration that consists of a black hole surrounded by a dark matter distribution. We then introduce the static line element via the anisotropic energy-momentum tensor containing tangential pressure P_θ used to describe the dark matter envelope. Afterwards, we review the definitions of flux, differential luminosity, and spectral luminosity as presented in the Novikov–Page–Thorne model. In Section 3, we solve the TOV equations and calculate the metric functions fulfilling boundary conditions in the different regions of spacetime. Then, we compute the angular velocity, energy, and angular momentum of the configuration and plot the modeled flux and luminosity spectrum for various values of the parameter related to the dark matter anisotropy. Implications of the model for astrophysical black hole candidates are then discussed in Section 4.

2. Black Hole Surrounded by Anisotropic Dark Matter

In the following we investigate a system composed of a static black hole with a dark matter envelope around it, where the dark matter is introduced only for the purpose of modifying the geometry around the black hole. Because the black hole represents the accretor, one can split the mass profile of the overall configuration into three regions,

$$M(r) = \begin{cases} M_{BH}, & r_g < r \leqslant r_b, \\ M_{BH} + M_{DM}(r), & r_b \leqslant r \leqslant r_s, \\ M_{BH} + M_{DM}(r_s), & r_s \leqslant r, \end{cases} \quad (1)$$

where $r_g = 2M_{BH}$ is the gravitational radius and M_{BH} is the mass of the black hole, whereas r_b and r_s are the inner and outer edges (radii) of the dark matter envelope. In particular, r_b corresponds to the boundary that separates the inner vacuum region from the outer distribution of dark matter. Accordingly, the above configuration can be described as follows:

1. the core is modeled by the accretor in the form of a black hole. Its mass, M_{BH}, is a free parameter of our model;
2. the black hole is surrounded by a dark matter shell that extends from a radius r_b up to the radius r_s;
3. at r_s, the dark matter mass reaches its maximum value $M_{DM}(r_s)$ and beyond r_s we assume vacuum;
4. at $r \geqslant r_s$ the total mass of the system is defined as $M_T = M(r_s)$.

To model the dark matter distribution in the shell, $r \in [r_b, r_s]$, we assume an exponential sphere profile of the form

$$\rho(r) = \rho_0 e^{-\frac{r}{r_0}}, \quad r \geqslant r_b, \quad (2)$$

where ρ_0 is the dark matter density at $r = 0$ and r_0 is the scale radius. The exponential density profile was introduced in Sofue (2013) to explain the rotation curve in the bulge of the Milky Way. Indeed, it showed a better fit of the observational data compared to the widely adopted de Vaucouleurs law in the inner part of the galaxy. Recently, it was also applied to study the effects of nonvanishing dark matter pressure in the entire Milky Way (Boshkayev et al. 2021a).

As a consequence, assuming spherical symmetry, the dark matter mass profile is given by

$$M_{DM}(r) = \int_{r_b}^{r} 4\pi \tilde{r}^2 \rho(\tilde{r}) \, d\tilde{r}, \quad (3)$$

which yields

$$M_{DM}(x) = 8\pi r_0^3 \rho_0 \left[e^{-x_b}\left(1 + x_b + \frac{x_b^2}{2}\right) \right.$$
$$\left. - e^{-x}\left(1 + x + \frac{x^2}{2}\right) \right], \quad (4)$$

for $r > r_b$, where we have substituted $x = r/r_0$ and $x_b = r_b/r_0$. For vanishing r_b, the profile (3) reduces to the one obtained in Sofue (2013).

2.1. TOV Equations with Anisotropic Pressure

To describe the physical properties of the system in Equation (1), we consider the spherically symmetric line element

$$ds^2 = e^{N(r)}dt^2 - e^{\Lambda(r)}dr^2 - r^2(d\theta^2 + \sin^2\theta d\varphi^2), \quad (5)$$

where, as usual, we take (t, r, θ, φ) as the time and spherical coordinates, respectively, while $N(r)$ and $\Lambda(r)$ represent the unknown metric functions.

The energy-momentum tensor is given by

$$T^{\alpha\beta} = (\rho + P_\theta)u^\alpha u^\beta - P_\theta g^{\alpha\beta} + (P - P_\theta)\chi^\alpha \chi^\beta, \quad (6)$$

where $u^\alpha u_\alpha = 1 = -\chi^\alpha \chi_\alpha$, $u^\alpha \chi_\alpha = 0$, $u^\alpha = e^{-N/2}\delta_0^\alpha$ is the four-velocity, and $\chi^\alpha = e^{-\Lambda/2}\delta_1^\alpha$ is a unit space-like vector in the radial direction, with δ_i^α the Kronecker symbol (Rahman-syah & Sulaksono 2021). Using Einstein's equations for the line element (5) and the energy-momentum tensor (6), we obtain the following expressions (Fayos et al. 1996):

$$\frac{dP(r)}{dr} = -(\rho(r) + P(r))\frac{M(r) + 4\pi r^3 P(r)}{r(r - 2M(r))}$$
$$+ \frac{2}{r}(P_\theta(r) - P(r)), \quad (7)$$

$$\frac{dN(r)}{dr} = 2\frac{M(r) + 4\pi r^3 P(r)}{r(r - 2M(r))}, \quad (8)$$

which generalize the TOV equations to the case of anisotropic pressures and relate the density, $\rho(r)$, with the radial pressure, $P(r)$, and the tangential term, $P_\theta(r)$. In general, this is a system of two equations in four unknowns, and therefore two functions must be provided in order to close it. Typically, this is done by

specifying the equations of state that relate the pressures $P_\theta(r)$ and $P(r)$ to the density. In our model, however, $\rho(r)$ is the dark matter density given by Equation (2), whereas $M(r)$ is given by Equation (1); therefore, these quantities are no longer unknown functions to be determined. Notice, however, that one unknown function remains to be specified. This function can be taken to be the pressure difference $P_\theta(r) - P(r)$, appearing in Equation (7), which is not known a priori.

A possible viable strategy to employ has been discussed in Horvat et al. (2011) and Folomeev & Dzhunushaliev (2015), where the anisotropy function, $\Delta(r)$, has been introduced as

$$\Delta(r) \equiv P_\theta(r) - P(r) = \alpha\mu(r)P(r), \qquad (9)$$

where α is a free constant, physically interpreted as the anisotropy parameter, while μ is the compactness of the system defined by

$$\mu(r) = \frac{2M(r)}{r} = 1 - e^{-\Lambda(r)}. \qquad (10)$$

In general, μ indicates the strength of the gravitational field. If $\mu \ll 1$ the field is weak, and if $\mu \sim 1$ the field is strong. An interesting characteristic of Equation (9) is that μ guarantees the required vanishing of the anisotropy of pressures at $r = 0$ (notice that typically $M(r) \sim r^3$ is close to the center). Moreover, in the weak-field limit, the anisotropy of pressure is not expected to be important. In addition, this ansatz makes sure that the tangential pressure vanishes at the surface of the object (Horvat et al. 2011), in our case at the surface of the dark matter envelope.

Notice that, according to Equation (9), $\alpha < 0$ corresponds to $P_\theta < P$, $\alpha = 0$ corresponds to the isotropic case $P_\theta = P$, and $\alpha > 0$ corresponds to $P_\theta > P$. The case of a static black hole surrounded by a dark matter envelope with isotropic pressures, i.e., $\alpha = 0$, has been studied in detail by some of us in Boshkayev et al. (2020) within a model that closely follows the one considered here.

Furthermore, to analyze our model, we should now establish the boundary conditions between the inner and outer solutions.

2.2. Boundary Conditions

As stated above, the innermost region is given by a black hole vacuum solution with the event horizon located at $r = r_g$, while the exterior region corresponds to the dark matter distribution extending from a radius $r_b > r_g$ to an outer radius $r_s > r_b$. The values of density, pressures, and metric functions at the boundary are determined from $\rho(r_b)$, $P(r_b)$, and $N(r_b)$. They can be computed immediately, obtaining

$$\rho(r_b) = \rho_b = \rho_0\, e^{-\frac{r_b}{r_0}}, \qquad (11)$$

$$P(r_b) = P_b, \qquad (12)$$

$$N(r_b) = N_b = \ln\left(1 - \frac{r_g}{r_b}\right). \qquad (13)$$

Consequently, the unknown metric functions, $N(r)$ and $\Lambda(r)$, are evaluated as

$$e^{N(r)} = \begin{cases} 1 - \dfrac{r_g}{r}, & r_g < r \leqslant r_b, \\[2mm] e^{N_r(r)}, & r_b \leqslant r \leqslant r_s, \\[2mm] 1 - \dfrac{2M(r_s)}{r}, & r_s \leqslant r, \end{cases} \qquad (14)$$

and

$$e^{\Lambda(r)} = \begin{cases} \left(1 - \dfrac{r_g}{r}\right)^{-1}, & r_g < r \leqslant r_b, \\[3mm] \left(1 - \dfrac{2M(r)}{r}\right)^{-1}, & r_b \leqslant r \leqslant r_s, \\[3mm] \left(1 - \dfrac{2M(r_s)}{r}\right)^{-1}, & r_s \leqslant r, \end{cases} \qquad (15)$$

where $N_r(r)$ is simply the function $N(r)$ in the interval $r \in [r_b, r_s]$, which must be numerically evaluated from the TOV equations fulfilling the corresponding boundary conditions.

It is worth noticing that if we follow this consolidated procedure for matching different spacetimes by imposing continuity of the first and second fundamental forms, the dark matter pressure should vanish when $r = r_b$. Therefore, the condition $P(r_b) = P_b$ leads to noncontinuous matching because the first derivatives of the metric show a jump at the boundary. However, there is a natural physical explanation for the discontinuity. The common interpretation is to assume the presence of a massive surface layer at r_b for which the three-dimensional energy-momentum can be evaluated from the matching conditions, as discussed in Israel (1966, 1967).

2.3. Radiative Flux and Spectral Luminosity

Bearing in mind the above results, we can now investigate the flux and spectral luminosity produced by an accretion disk in the geometry with the above proposed ansatz. The disk extends from an inner edge r_i, which is usually taken as the innermost stable circular orbit (ISCO) for test particles, $r_i = r_{\rm ISCO}$. To this end, we follow the simple approach proposed by Novikov–Thorne and Page–Thorne in Novikov & Thorne (1973) and Page & Thorne (1974) and write the radiative flux $\mathcal{F}$ as

$$\mathcal{F}(r) = -\frac{\dot{m}}{4\pi\sqrt{g}} \frac{\Omega_{,r}}{(E - \Omega L)^2} \int_{r_i}^{r} (E - \Omega L)L_{,\tilde{r}} d\tilde{r}. \qquad (16)$$

The above quantity depends upon $\dot{m}$, i.e., the disk mass accretion rate, which is unknown. In the simplest case, we can take it as constant, and we can set $\dot{m} = 1$, which is equivalent to considering the normalized flux per unit accretion rate, i.e., $\mathcal{F}(r)/\dot{m}$. Moreover, g is the determinant of the three-dimensional subspace with coordinates (t, r, φ) and is given by $\sqrt{g} = \sqrt{g_{\rm tt}g_{\rm rr}g_{\varphi\varphi}}$. The quantities appearing in Equation (16) are

$$\Omega(r) = \frac{d\varphi}{dt} = \sqrt{-\frac{\partial_r g_{\rm tt}}{\partial_r g_{\varphi\varphi}}}, \qquad (17)$$

$$E(r) = u_t = u^t g_{\rm tt}, \qquad (18)$$

$$L(r) = -u_\varphi = -u^\varphi g_{\varphi\varphi} = -\Omega u^t g_{\varphi\varphi}, \qquad (19)$$
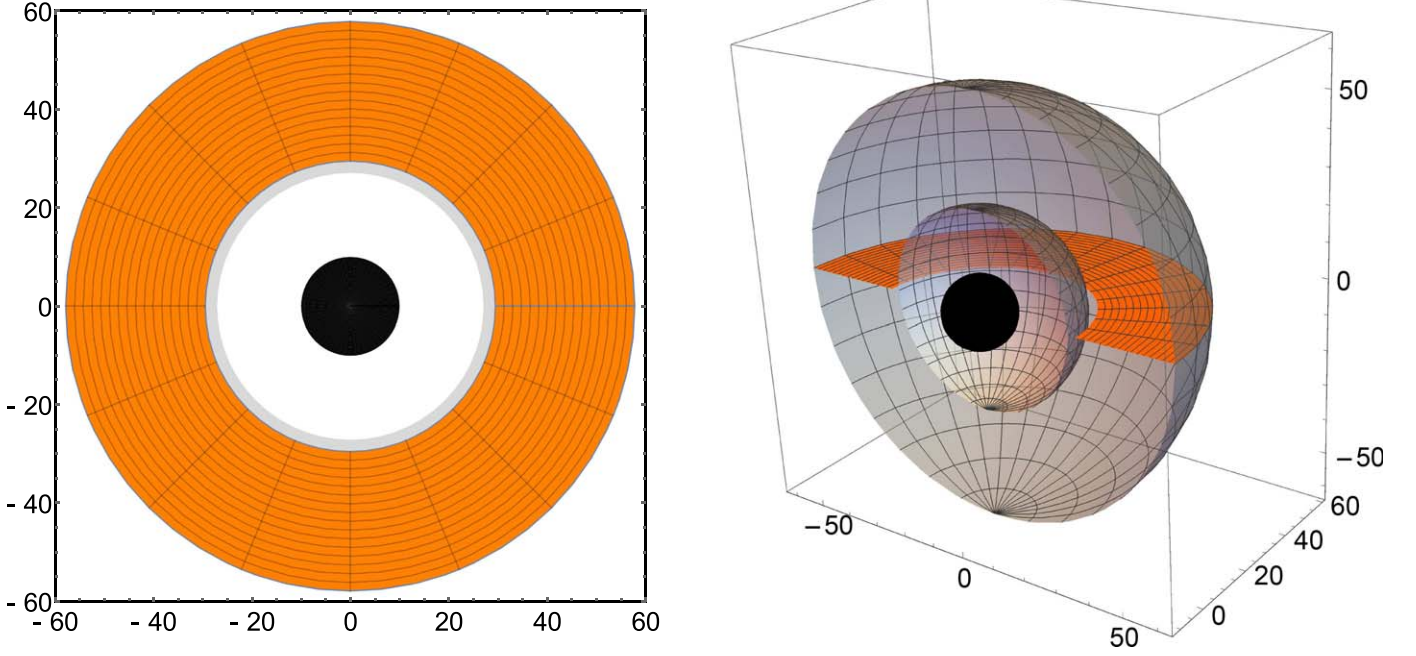
Figure 1. Left panel: two-dimensional schematic illustration of the system at the equatorial plane. The central black disk represents a black hole of radius $r_g = 2M_{\mathrm{BH}} = 10^9 M_\odot \approx 9.866$ au, the gray disk shows the dark matter distribution starting from $r_b = 27.133$ au up to $r_s = 57.755$ au, and the orange disk represents an accretion disk of inner radius $r_{\mathrm{ISCO}} = 29.414$ au and outer radius r_s. Right panel: the cross section of the three-dimensional plot. The black sphere is the black hole, the dark matter distribution is confined within the two gray spheres of radii r_b and r_s, and the accretion disk is at the equatorial plane.

$$u^t(r) = \dot{t} = \frac{1}{\sqrt{g_{\mathrm{tt}} + \Omega^2 g_{\varphi\varphi}}}, \qquad (20)$$

namely $\Omega = \Omega(r)$ is the orbital angular velocity, $E = E(r)$ is the energy per unit mass, and $L = L(r)$ is the orbital angular momentum per unit mass of the test particle. Additionally, ∂_r is the derivative with respect to the radial coordinate r, a dot represents the derivative with respect to the proper time, and u^t is the time component of the 4-velocity.

Another important quantity is the differential luminosity that is interpreted as the energy per unit of time reaching an observer at infinity. We denote it by $\mathcal{L}_\infty$ and estimate it through the flux, $\mathcal{F}$, by means of the following relation (Novikov & Thorne 1973; Page & Thorne 1974):

$$\frac{d\mathcal{L}_\infty}{d\ln r} = 4\pi r \sqrt{g} E \mathcal{F}(r). \qquad (21)$$

If the radiation emission is assumed to be well described by a blackbody, then we can express the spectral luminosity at infinity $\mathcal{L}_{\nu,\infty}$ as a function of the radiation's frequency ν (Boshkayev et al. 2020):

$$\nu \mathcal{L}_{\nu,\infty} = \frac{60}{\pi^3} \int_{r_i}^\infty \frac{\sqrt{g} E}{M_T^2} \frac{(u^t y)^4}{\exp[u^t y / \mathcal{F}^{*1/4}] - 1} dr, \qquad (22)$$

where $y = h\nu/kT_*$, h is Planck's constant, k is Boltzmann's constant, M_T is the total mass, $\mathcal{F}^* = M_T^2 \mathcal{F}$, and we have taken $r_i = r_{\mathrm{ISCO}}$. Also, T_* is the characteristic temperature defined from the Stefan–Boltzmann law, which reads

$$\sigma T_* = \frac{\dot{m}}{4\pi M_T^2}, \qquad (23)$$

with σ the Stefan–Boltzmann constant.

To compare with a Schwarzschild black hole in a vacuum, it is also interesting to calculate the radiative efficiency of the source, i.e., the amount of rest-mass energy of the disk that is converted into radiation, which is given by

$$\mathcal{L}_\infty / \dot{m} = 1 - E(r_{\mathrm{ISCO}}), \qquad (24)$$

which in the case of a Schwarzschild black hole gives the known result $\eta = (1 - E(r_{\mathrm{ISCO}})) \times 100\% \simeq 5.7\%$.

In Figure 1 we show a schematic representation of the system examined here. The left panel presents a two-dimensional diagram of the equatorial plane of the system, whereas the right panel shows a cross section of the three-dimensional diagram. One can see that $r_b < r_{\mathrm{ISCO}} < 3r_g$. Thus, the presence of dark matter alters the geometry around a black hole and decreases the value of r_{ISCO}.

3. Discussion of Numerical Results

To compute the orbital parameters of the test particles, the flux, and the differential and spectral luminosities of an accretion disk, we need first to numerically solve the TOV equations. The corresponding numerical solutions for the pressure and metric functions must fulfill the boundary conditions above reported in Equations (14)–(15). In particular, holding $P(r) = 0$ at $r = r_s$, i.e., at the surface radius of the dark matter envelope, implies that N and Λ have to ensure $N(r_s) = -\Lambda(r_s)$ on the surface. However, the numerical value of the function $N(r)$, which is denoted $N_n(r_s)$, obtained from the numerical solution of the TOV equations, is not equal to $-\Lambda(r_s)$. This is related to the fact that the boundary condition $N(r_b) = \ln(1 - r_g/r_b)$ is imposed while solving the TOV equations, whereas the boundary condition $N(r_s) = \ln(1 - 2M(r_s)/r_s)$ is not. Therefore, in order to satisfy the latter boundary condition, one needs a redefinition of the function N_n. The most suitable redefinition of N_n is the

Table 1
Physical Parameters of the Dark Matter Envelope with Fixed
$\rho_0 = 0.85 \times 10^{-5}$ au^{-2} and $P_b = 2.356 \times 10^{-8}$ au^{-2}

α	r_{ISCO} (r_T)	r_s (r_T)	$10^{-2}M_{\text{DM}}(r_s)$ (M_T)	M_T ($10^8\,M_\odot$)	η (%)
-0.10	2.928	5.750	1.7761957	5.0904157	5.866
-0.08	2.925	5.912	1.8099900	5.0921677	5.856
-0.06	2.921	6.124	1.8488401	5.0941833	5.845
-0.04	2.916	6.427	1.8954049	5.0966012	5.830
-0.02	2.909	6.957	1.9561495	5.0997589	5.808
-0.01	2.903	7.498	1.9982066	5.1019474	5.789
-10^{-3}	2.891	9.359	2.0609501	5.1052160	5.747
-10^{-5}	2.882	13.268	2.0786001	5.1061361	5.706
-10^{-7}	2.879	17.343	2.0792547	5.1061703	5.686
-10^{-9}	2.876	21.534	2.0792725	5.1061712	5.674
0	2.875	24.086	2.0792729	5.1061712	5.670
6.78×10^{-11}	2.874	28.626	2.0792729	5.1061712	5.664
6.85×10^{-11}	2.874	29.726	2.0792730	5.1061712	5.662
6.887×10^{-11}	2.872	39.936	2.0792730	5.1061712	5.655

Note. In addition, the black hole mass $M_{\text{BH}} = 5 \times 10^8\,M_\odot \approx 4.933$ au, the corresponding gravitational radius $r_g = 2M_{\text{BH}}$, the inner edge of the dark matter envelope $r_b = 5.5M_{\text{BH}}$ are the model free parameters and therefore are also fixed. The choice of the anisotropic parameter α determines the innermost stable circular orbit radius r_{ISCO}, the radius of the dark matter envelope r_s, and its total mass $M_{\text{DM}}(r_s)$. The first column shows various values of α, the second r_{ISCO} in units of the gravitational radius r_T corresponding to the total mass of the system $M_T = r_T/2$, the third r_s in units of r_T, the fourth $M_{\text{DM}}(r_s)$ in units of M_T, the fifth M_T in units of solar mass, and the sixth the radiative efficiency of the source $\eta = (1 - E(r_{\text{ISCO}})) \times 100\%$.

following:

$$N_r(r) = N_n(r) - \left[N_n(r_s) - \ln\left(1 - \frac{2M(r_s)}{r_s}\right) \right]$$
$$\times \frac{r - r_b}{r_s - r_b}, \tag{25}$$

which clearly fulfills the boundary conditions in Equation (14).

The numerical analysis that follows shows that the effects of the presence of the dark matter envelope depend on the value of the parameter α in Equation (9). It is worth noticing that in order to solve the TOV equations, one needs to restrict α to negative or small positive values. The outer boundary of the envelope r_s is determined from the TOV equations by imposing $P(r_s) = 0$, once ρ_0, P_b and α are fixed. Finally, the total amount of dark matter in the envelope is given by $M_{\text{DM}}(r_s)$. With these ingredients, we fully determine the metric functions, and therefore, we can study the motion of test particles within the dark matter cloud under the hypothesis that dark matter does not interact with the baryonic matter of the accretion disk, and therefore, test particles move on geodesics in the geometry produced by the dark matter envelope surrounding the black hole. The value of r_{ISCO} is obtained from the evaluation of stable circular orbits within the dark matter envelope, and it is set as the inner edge of the disk.

A comparison of the values of r_s, M_{DM}, and r_{ISCO} for different values of α can be found in Table 1.

It is worth noticing that, for a fixed value of ρ_0 and P_b, the TOV equations can be solved for a wide range of values of $\alpha < 0$, which implies $P_\theta < P$. On the other hand, for $\alpha > 0$, i.e., $P_\theta > P$, there are maxima of α for which the TOV equations lead to unstable dark matter configurations and the TOV equations will not have solutions. Also, the total dark matter mass tends to reach a maximum value of $M_{\text{DM}}(r_s) \simeq 2.12342 \times 10^{-2}\,M_{\text{BH}}$ for $\alpha \simeq -10^{-8} \div 10^{-9}$. Similarly, considering a central black hole of mass $M_{\text{BH}} = 5 \times 10^8\,M_\odot \approx 4.933$ au (with $M_\odot$ being the mass of the Sun), the value of α affects only slightly the location of the ISCO, while it affects significantly the outer edge of the envelope r_s, i.e., r_s and $M_{\text{DM}}(r_s)$ increase with increasing α from negative to positive values. On the contrary, the radiative efficiency of the accretion disk decreases as α increases. See Table 1 for details.
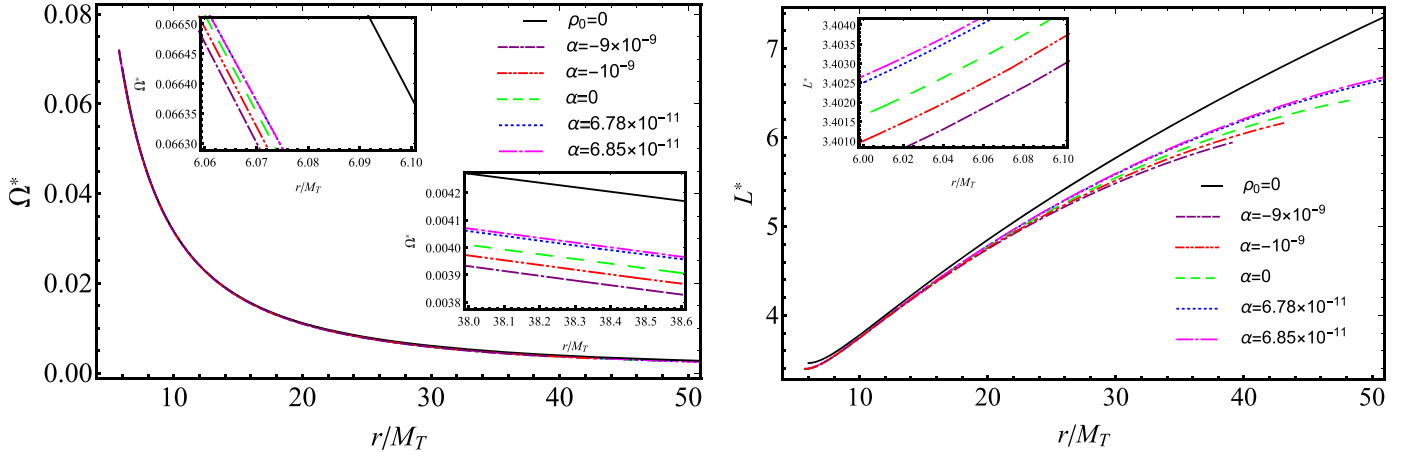
Figure 2. Left panel: numerical evaluation of the orbital angular velocity Ω^* of test particles in the accretion disk around a static black hole of mass $M_{\text{BH}} = 5 \times 10^8\,M_\odot \approx 4.933$ au in the presence of anisotropic dark matter as a function of r/M_T. Right panel: numerical evaluation of the orbital angular momentum L^* of test particles in the accretion disk as a function of r/M_T. In both figures, the solid black curves represent the case of a static black hole without dark matter while the other curves represent anisotropic dark matter envelopes with $\rho_0 = 0.85 \times 10^{-5}$ au^{-2}.
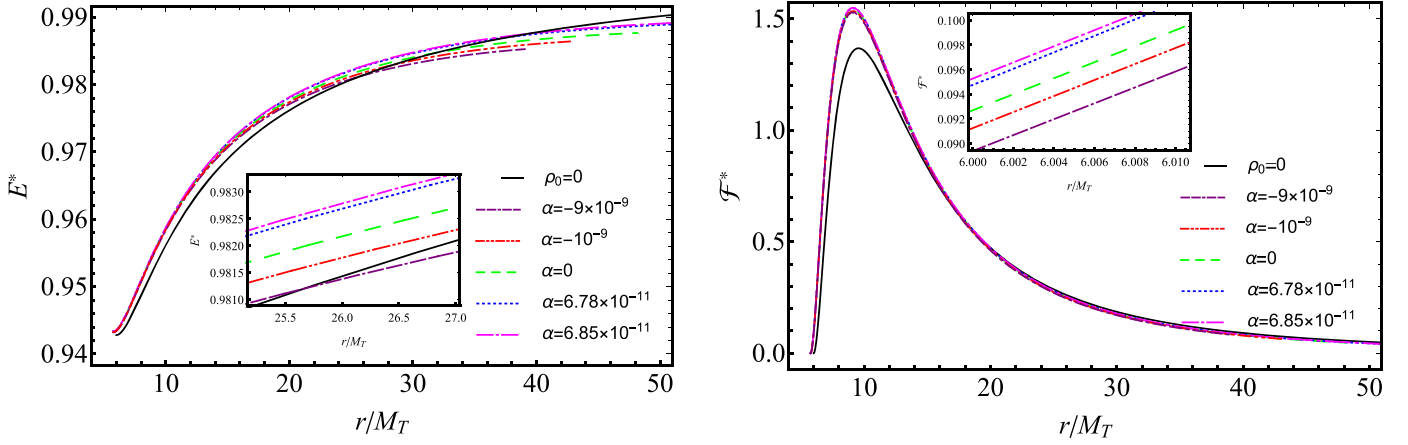
Figure 3. Left panel: numerical evaluation of energies E^* of test particles in the accretion disk around a static black hole of mass $M_{\mathrm{BH}} = 5 \times 10^8\, M_\odot \approx 4.933$ au in the presence of anisotropic dark matter as a function of r/M_T. Right panel: numerical evaluation of the flux $\mathcal{F}$ divided by 10^{-5} of the accretion disk as a function of r/M_T. In both figures, the solid black curves represent the case of a static black hole without dark matter while the other curves represent anisotropic dark matter envelopes with $\rho_0 = 0.85 \times 10^{-5}$ au^{-2}.
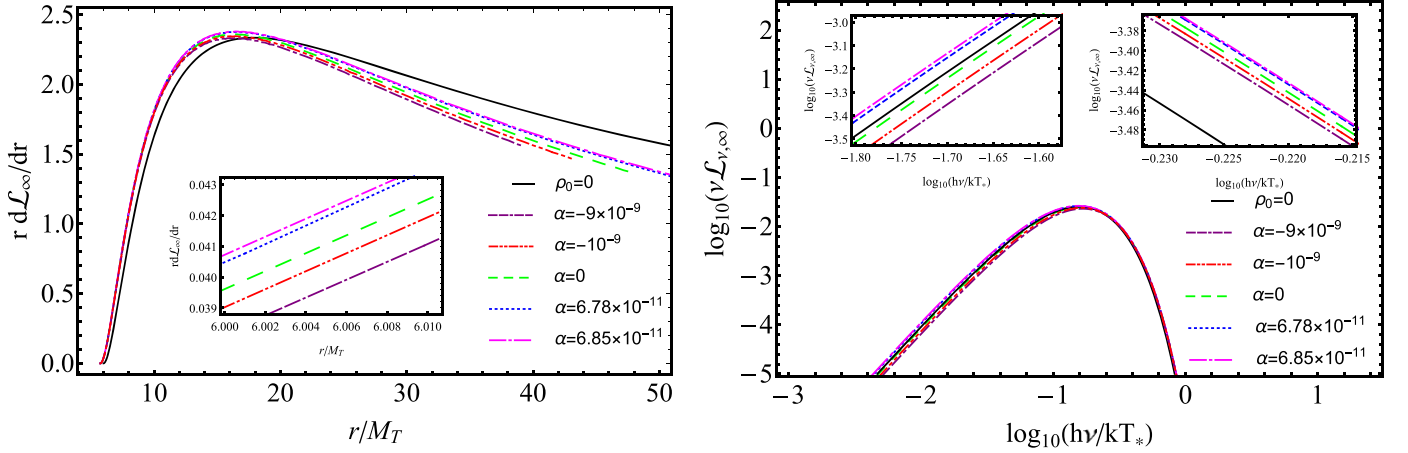
Figure 4. Left panel: numerical evaluation of the differential luminosity of the accretion disk scaled in powers of 10^{-2} as a function of r/M_T. Right panel: numerical evaluation of the spectral luminosity of the accretion disk as a function of $h\nu/kT_*$, i.e., as a function of frequency. In both figures, the solid curves represents the case of a static black hole without dark matter. The intersection points are listed in Table 2.

With the above numerical setup, in Figure 2 we plot $\Omega^\star = M_T\Omega$ and $L^\star = L/M_T$, i.e., the dimensionless orbital angular velocity and orbital angular momentum of test particles in the presence of a dark matter envelope, as functions of r/M_T. The solid curves represent the case of a static black hole without dark matter, namely, $\rho_0 = 0$, and are easily distinguished from the other curves. For other curves, the values of density and pressure are fixed as $\rho_0 = 0.85 \times 10^{-5}$ au^{-2} and $P_b = 2.356 \times 10^{-8}$ au^{-2}, and α is varied. In particular, the distinction is more marked for the orbital angular momentum $L^\star$, especially for large values of r/M_T.

Similar plots for $E^\star$ and $\mathcal{F}^\star$, namely, the energy per unit mass of test particles and the disk's flux, are obtained in Figure 3. In the case of energy, one can see that for smaller r/M_T, $E^\star$ is larger than the pure vacuum case while it becomes smaller as r/M_T increases. Consequently, for each α, there is an intersection point of the $\rho_0 = 0$ curve with the $\rho_0 = 0.85 \times 10^{-5}$ au^{-2} curve, which produces the same energy. In the case of flux, it is noticeable that the presence of anisotropic dark matter with different α increases the maximum compared to the $\rho_0 = 0$ case.

The differential luminosity as a function of r/M_T is reported in the left panel of Figure 4. The numerical evaluation is scaled in powers of 10^{-2} and shows how the absence of dark matter produces lower luminosity compared to the case with dark matter for small radii up to $r/M_T \simeq 15$, and higher luminosity for larger values of r/M_T. This suggests that the accretion disk in the presence of dark matter should emit more energy compared to the accretion disk in vacuum for high frequencies, as can be seen from the right panel of Figure 4, which shows the spectral luminosity of the accretion disk as a function of the radiation frequency in a log–log plot. In fact, all frequency ranges for $\alpha > 0$ possess higher luminosity compared to the $\rho_0 = 0$ case, i.e., Schwarzschild. However, for $\alpha \leqslant 0$, the situation is different and at lower frequencies, the luminosity is lower and at higher frequencies the luminosity is higher than the Schwarzschild case.

It is relevant to note that, although our approach is model dependent because it relies on the assumptions made on compactness—see Equation (9)—the various possible values of α do not impact significantly on the physics of the disk's emission. This can be seen from the fact that the cases with anisotropic pressures are similar to each other and to the isotropic case, i.e., $\alpha = 0$, when compared with the vacuum case (solid line in the plots), suggesting that the effects on the
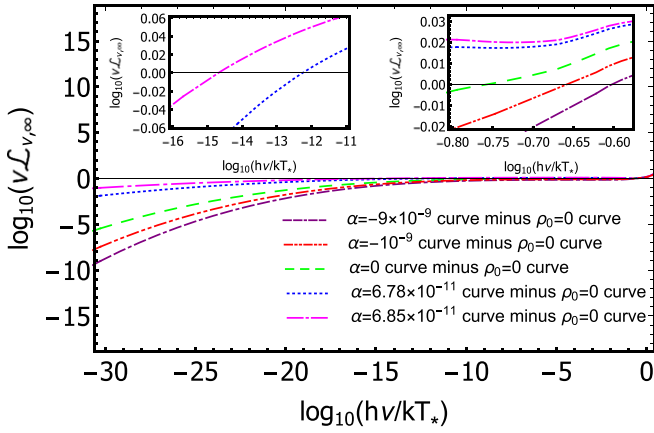
Figure 5. The difference of the spectral luminosity of the accretion disk between different α curves (with fixed $\rho_0 = 0.85 \times 10^{-5}$ au^{-2} and $P_b = 2.356 \times 10^{-8}$ au^{-2}) and the vacuum case, i.e., $\rho_0 = 0$.

Table 2
Intersection Points between Several Luminosity Curves with $\rho_0 = 0.85 \times 10^{-5}$ au^{-2} and $P_b = 2.356 \times 10^{-8}$ au^{-2} and Different Values of α and the Luminosity Curve of a Schwarzschild Black Hole in Vacuum $\rho_0 = 0$

α	$\log_{10}(h\nu/kT_*)$	$\log_{10}(\nu\mathcal{L}_{\nu,\infty})$
-9×10^{-9}	-0.603	-1.764
-10^{-9}	-0.651	-1.670
0	-0.756	-1.606
6.78×10^{-11}	-12.254	-33.397
6.85×10^{-11}	-14.683	-39.156

Note. The first column shows the different values of α considered. The second and third columns show the frequencies of the emitted radiation and the spectral luminosity illustrated in Figure 5.

spectrum are due mostly to the presence of dark matter rather than to the possible anisotropies.

From an experimental perspective, in principle, it would be possible to obtain information about the presence of dark matter from the spectra of accretion disks, if the other relevant quantities, such as the black hole mass and the disk's ISCO, can be determined independently. Last but not least, it is important to remember that even the observable properties of the dark matter distribution are also model dependent because they rely on the choice made in Equation (2). Although the choices of different density profiles in Equation (2) and equations of state and prescriptions for the anisotropies in Equation (9) would modify the values of quantities such as r_{ISCO} and the flux of the accretion disk, we may expect that the overall qualitative features due to the presence of dark matter would remain unchanged.

The case when $\alpha = 0$, or $P_\theta = P$, has been considered in Boshkayev et al. (2020). In principle, one can expect that tangential pressures alone, i.e., in the absence of radial pressures, also known as an "Einstein cluster" (Einstein 1939; Gilbert 1954; Hogan 1973), could also reproduce analogous results providing de facto a degeneracy between the different approaches. The case of vanishing radial pressures is interesting in itself as it may approximate a rotating fluid while keeping the advantage of making the equations much easier, and it has been used to model the properties of dark matter halos in Böhmer and Harko (2007). The observational features of accretion disks in the Einstein cluster will appear in a separate article (K. Boshkayev 2022, in preparation.).
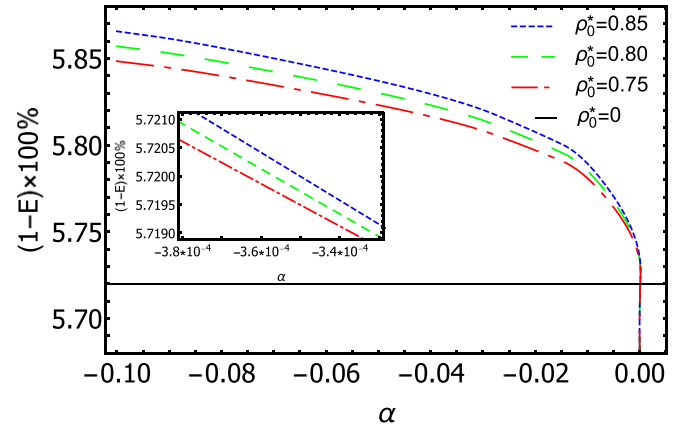
For the sake of clarity, in Figure 5 we show the difference in luminosity between the $\rho_0 = 0$ (Schwarzschild) case and the cases with different values of α (with fixed $\rho_0 = 0.85 \times 10^{-5}$ au^{-2} and $P_b = 2.356 \times 10^{-8}$ au^{-2}). The intersection points indicate that there exist frequencies for which the $\rho_0 \neq 0$ case with various α can mimic the Schwarzschild case. However, the overall spectrum for the cases in the presence of dark matter differs from that of the Schwarzschild case, and the deviation, which appears to be larger at smaller frequencies, may help constrain the values of α and ρ_0 from observations.

In Table 2 we show numerical values of the intersection points illustrated in Figure 5. For fixed $\rho_0 = 0.85 \times 10^{-5}$ au^{-2} and $P_b = 2.356 \times 10^{-8}$ au^{-2} and increasing values of α, the difference in luminosity decreases and so does the frequency.

Figure 6. Efficiency $\eta = (1 - E(r_{\text{ISCO}})) \times 100\%$ vs. α. The black solid line corresponds to the efficiency of the Schwarzschild black hole. The color curves show the efficiency in the presence of dark matter with different densities.

These numbers show the frequency at which the disk surrounding a Schwarzschild black hole in a vacuum can be mimicked by that of a black hole surrounded by dark matter with a given value of α.

Finally, in Figure 6 we plot the efficiency of the source as a function of α for different densities $\rho_0^* = 0.85, 0.80$, and 0.75, where $\rho_0^* = \rho_0/(10^{-5}$ au$^{-2})$. It is evident that a negative α will yield a larger efficiency compared to the Schwarzschild black hole in vacuum (5.72%) and for a positive α, the efficiency will be slightly smaller than 5.72%. For numerical values of the efficiency, see Table 1.

4. Final Outlooks

We considered a spherically symmetric configuration composed of a central black hole surrounded by a spherical dark matter envelope with anisotropic pressures. We studied the spectra produced by the accretion disk surrounding the central object assuming that the baryonic matter in the disk does not interact with the dark matter particles in the envelope.

Under a series of assumptions for the dark matter component of the system, namely the density profile, anisotropies, and inner boundary, we solved the TOV equations to determine the geometry inside the dark matter envelope and consequently the motion of test particles within the disk. We then numerically evaluated the flux and luminosity of the disk in the presence of

dark matter and compared it with the isotropic case and the vacuum case.

We showed that there exist frequencies in the spectrum of the accretion disk that bear the mark of the presence of dark matter and that are also affected by the anisotropies. This suggests that if other relevant quantities, such as the mass of the central black hole and the ISCO, can be determined independently, it could be possible, at least in principle, to distinguish different cases. In addition, we also estimated how the radiative efficiency of the source is affected by the presence of dark matter anisotropies and found that the efficiency increases compared to that of a Schwarzschild black hole immersed in isotropic dark matter when $P_\theta < P$.

Of course, the scenario presented here is just a simple toy model to highlight the qualitative features that the presence of anisotropies may bear on the accretion disk's spectrum. Astrophysical black holes are expected to be rotating and, therefore, the assumption of staticity, while simplifying the equations, is not particularly realistic. However, we expect similar results to hold in the presence of rotation of the central object, and we aim to investigate those in future works.

At present, our knowledge of the dark matter distribution near the center of galaxies is very limited, with most studies providing estimates for the dark matter density at distances of the order of several parsecs from the galactic center in the Milky Way. Similar estimates for other galaxies are missing. Similarly, we still do not know whether the geometry near compact objects at the center of galaxies is well described by the Kerr metric. We showed here that the presence of dark matter may affect the spectrum of the black hole's accretion disk and, therefore, provide valuable information on the nature of dark matter itself. The hope is that future observations will allow us to test such ideas and further constrain the properties of viable dark matter candidates.

ORCID iDs

K. Boshkayev https://orcid.org/0000-0002-1385-270X

D. Malafarina https://orcid.org/0000-0002-8100-8797

References

Abramowicz, M. A., Czerny, B., Lasota, J. P., & Szuszkiewicz, E. 1988, ApJ, 332, 646
Abramowicz, M. A., & Fragile, P. C. 2013, LRR, 16, 1
Bayin, S. S. 1982, PhRvD, 26, 1262
Böhmer, C. G., & Harko, T. 2007, MNRAS, 379, 393
Boshkayev, K., Idrissov, A., Luongo, O., & Malafarina, D. 2020, MNRAS, 496, 1115
Boshkayev, K., Konysbayev, T., Kurmanov, E., et al. 2021a, MNRAS, 508, 1543
Boshkayev, K., Konysbayev, T., Kurmanov, E., et al. 2021b, PhRvD, 104, 084009
Capozziello, S., D'Agostino, R., & Luongo, O. 2019, IJMPD, 28, 1930016
Capozziello, S., Luongo, O., & Mauro, L. 2021, EPJP, 136, 167
Copeland, E. J., Sami, M., & Tsujikawa, S. 2006, IJMPD, 15, 1753
Dai, D.-C., & Stojkovic, D. 2019, PhRvD, 100, 083513
DeBenedictis, A., Horvat, D., Ilijić, S., Kloster, S., & Viswanathan, K. S. 2006, CQGra, 23, 2303
Einstein, A. 1939, AnMat, 40, 922
Fayos, F., Senovilla, J. M. M., & Torres, R. 1996, PhRvD, 54, 4862
Folomeev, V., & Dzhunushaliev, V. 2015, PhRvD, 91, 044040
Gilbert, C. 1954, MNRAS, 114, 628
Guzmán, F. S. 2006, PhRvD, 73, 021501
Hartle, J. B., & Thorne, K. S. 1968, ApJ, 153, 807
Herrera, L., di Prisco, A., Martin, J., et al. 2004, PhRvD, 69, 084026
Herrera, L., Martin, J., & Ospino, J. 2002, JMP, 43, 4889
Herrera, L., Ospino, J., & di Prisco, A. 2008, PhRvD, 77, 027502
Ho, L. C., Filippenko, A. V., & Sargent, W. L. W. 1997, ApJ, 487, 568
Hogan, P. A. 1973, PRIAA, 73, 91
Horvat, D., Ilijić, S., & Marunović, A. 2011, CQGra, 28, 025009
Israel, W. 1966, NCimB, 44, 1
Israel, W. 1967, NCimB, 48, 463
Luongo, O., & Muccino, M. 2018, PhRvD, 98, 103520
Mak, M. K., & Harko, T. 2003, RSPSA, 459, 393
Mazur, P. O., & Mottola, E. 2004, PNAS, 101, 9545
Novikov, I. D., & Thorne, K. S. 1973, Black Holes (Les Astres Occlus) (New York: Gordon & Breach), 343
Page, D. N., & Thorne, K. S. 1974, ApJ, 191, 499
Paschalidis, V., & Stergioulas, N. 2017, LRR, 20, 7
Rahmansyah, A., & Sulaksono, A. 2021, J. Phys. Conf. Ser., 1816, 012025
Richstone, D., Ajhar, E. A., Bender, R., et al. 1998, Natur, 385, A14
Shapiro, S. L., & Teukolsky, S. A. 1983, Black Holes, White Dwarfs, and Neutron Stars: The Physics of Compact Objects (New York: Wiley)
Sofue, Y. 2013, PASJ, 65, 118
Torres, D. F. 2002, NuPhB, 626, 377